VEEGAN: Reducing Mode Collapse in GANs using Implicit Variational Learning

Akash Srivastava
School of Informatics
University of Edinburgh
akash.srivastava@ed.ac.uk

Lazar Valkov
School of Informatics
University of Edinburgh
L.Valkov@sms.ed.ac.uk

Chris Russell
The Alan Turing Institute
London
crussell@turing.ac.uk

Michael Gutmann
School of Informatics
University of Edinburgh
Michael.Gutmann@ed.ac.uk

Charles Sutton
School of Informatics & The Alan Turing Institute
University of Edinburgh
csutton@inf.ed.ac.uk

Abstract

Deep generative models provide powerful tools for distributions over complicated manifolds, such as those of natural images. But many of these methods, including generative adversarial networks (GANs), can be difficult to train, in part because they are prone to mode collapse, which means that they characterize only a few modes of the true distribution. To address this, we introduce VEEGAN, which features a reconstructor network, reversing the action of the generator by mapping from data to noise. Our training objective retains the original asymptotic consistency guarantee of GANs, and can be interpreted as a novel autoencoder loss over the noise. In sharp contrast to a traditional autoencoder over data points, VEEGAN does not require specifying a loss function over the data, but rather only over the representations, which are standard normal by assumption. On an extensive set of synthetic and real world image datasets, VEEGAN indeed resists mode collapsing to a far greater extent than other recent GAN variants, and produces more realistic samples.

1 Introduction

Deep generative models are a topic of enormous recent interest, providing a powerful class of tools for the unsupervised learning of probability distributions over difficult manifolds such as natural images [6, 10, 18]. Deep generative models are usually implicit statistical models [3], also called implicit probability distributions, meaning that they do not induce a density function that can be tractably computed, but rather provide a simulation procedure to generate new data points. Generative adversarial networks (GANs) [6] are an attractive such method, which have seen promising recent successes [17, 20, 23]. GANs train two deep networks in concert: a generator network that maps random noise, usually drawn from a multi-variate Gaussian, to data items; and a discriminator network that estimates the likelihood ratio of the generator network to the data distribution, and is trained

using an adversarial principle. Despite an enormous amount of recent work, GANs are notoriously fickle to train, and it has been observed [1, 19] that they often suffer from *mode collapse*, in which the generator network learns how to generate samples from a few modes of the data distribution but misses many other modes, even though samples from the missing modes occur throughout the training data.

To address this problem, we introduce VEEGAN,[1] a variational principle for estimating implicit probability distributions that avoids mode collapse. While the generator network maps Gaussian random noise to data items, VEEGAN introduces an additional *reconstructor* network that maps the true data distribution to Gaussian random noise. We train the generator and reconstructor networks jointly by introducing a implicit variational principle, which involves a novel upper bound on the cross-entropy between the reconstructor network and the original noise distribution of the GAN. Our objective function combines the traditional discriminator with an autoencoder of the noise vectors — thus providing an additional, complementary learning signal that avoids mode collapse.

Unlike other adversarial methods that train reconstructor networks [4, 5, 22], the noise autoencoder dramatically reduces mode collapse. Unlike recent adversarial methods that also make use of a data autoencoder [1, 12, 14], VEEGAN autoencodes noise vectors rather than data items. This is a significant difference, because choosing an autoencoder loss for images is problematic, but for Gaussian noise vectors, an ℓ_2 loss is entirely natural. Experimentally, on both synthetic and real-world image data sets, we find that VEEGAN is dramatically less susceptible to mode collapse, and produces higher-quality samples, than other state-of-the-art methods.

2 Background

Implicit probability distributions are specified by a sampling procedure, but do not have a tractable density [3]. Although a natural choice in many settings, implicit distributions have historically been seen as difficult to estimate. However, recent progress in formulating density estimation as a problem of supervised learning has allowed methods from the classification literature to enable implicit model estimation, both in the general case [9] and for deep generative adversarial networks (GANs) in particular [6]. Let $\{x_i\}_{i=1}^N$ denote the training data, where each $x_i \in \mathbb{R}^D$ is drawn from an unknown distribution $p(x)$. A GAN is a neural network G_γ that maps representation vectors $z \in \mathbb{R}^K$, typically drawn from a standard normal distribution, to data items $x \in \mathbb{R}^D$. Because this mapping defines an implicit probability distribution, training is accomplished by introducing a second neural network D_ω, called a discriminator, whose goal is to distinguish samples from the generator to those from the data. The parameters of these networks are estimated by solving the minimax problem

$$\max_\omega \min_\gamma \mathcal{O}_{\text{GAN}}(\omega, \gamma) := E_z \left[\log \sigma \left(D_\omega(G_\gamma(z))\right)\right] + E_x \left[\log \left(1 - \sigma \left(D_\omega(x)\right)\right)\right],$$

where E_z indicates an expectation over the standard normal z, E_x indicates an expectation over the empirical distribution, and σ denotes the sigmoid function. At the optimum, in the limit of infinite data and arbitrarily powerful networks, we will have $D_\omega = \log q_\gamma(x)/p(x)$, where q_γ is the density that is induced by running the network G_γ on normally distributed input, and hence that $q_\gamma = p$ [6].

Unfortunately, GANs can be difficult and unstable to train [19]. One common pathology that arises in GAN training is mode collapse, which is when samples from $q_\gamma(x)$ capture only a few of the modes of $p(x)$. An intuition behind why mode collapse occurs is that the only information that the objective function provides about γ is mediated by the discriminator network D_ω. For example, if D_ω is a constant, then $\mathcal{O}_{\text{GAN}}$ is constant with respect to γ, and so learning the generator is impossible. When this situation occurs in a localized region of input space, for example, when there is a specific type of image that the generator cannot replicate, this can cause mode collapse.

3 Method

The main idea of VEEGAN is to introduce a second network F_θ, which we call the *reconstructor network*, which learns the reverse feature mapping from data items x to representations z. To understand why this might prevent mode collapse, consider the example in Figure 1. In both columns of the figure, the middle vertical panel represents the data space, where in this example the true

[1] VEEGAN is a Variational Encoder Enhancement to Generative Adversarial Networks.

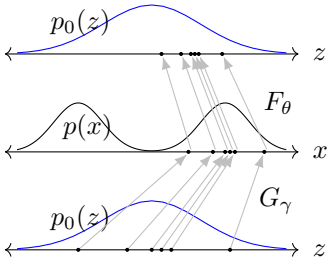

(a) A good choice of F_θ can help to detect mode collapse, when $F_\theta(G_\gamma(Z))$ is non-Gaussian.

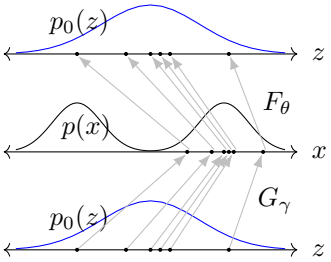

(b) A poor choice of F_θ could fail to detect mode collapse.

Figure 1: Illustration of how a reconstructor network F_θ can help to detect mode collapse in a deep generative network G_γ. The data distribution is $p(x)$ and the Gaussian is $p_0(z)$. See text for details.

distribution $p(x)$ is a mixture of two Gaussians. The bottom panel depicts the input to the generator, which is drawn from a standard normal distribution, and depicts the action of the generator network G_γ. In this example, the generator has captured only one of the two modes of $p(x)$. Now, starting from Figure 1a, we might intuitively hope that because the generated data points are highly concentrated in data space, F_θ will map them to a small range in representation space, as shown in the top panel of Figure 1a. This would then allow us to detect mode collapse, and hence provide a learning signal for γ, because the points in representation space do not appear to be drawn from a standard normal.

However, if we wish to detect mode collapse, we must choose F_θ carefully. In this example, a poor choice of F_θ is shown in Figure 1b. Now applying $F_\theta \circ G_\gamma$ to the generator input returns samples that appear to be drawn from a standard normal, so F_θ is no help in detecting this example of mode collapse. To address this problem, we need an appropriate learning principle for θ, which we introduce in the next section.

3.1 Objective Function

Here we present the learning objective used in VEEGAN. We draw on the intuition that the reconstructor should aim to reverse the operation of the optimal generator. The generator network G_γ implicitly defines a distribution $q_\gamma(x)$, which we can simulate by sampling from the random vector $G_\gamma(Z)$, where $Z \sim \mathcal{N}(0, I)$. In other words, the generator can be seen as attempting to map a standard normal random vector Z to the data vector X. Our key insight is to train F_θ to reverse this process. That is, we interpret F_θ as defining an implicit distribution $p_\theta(z)$ over representations, and choose F_θ to map the data distribution to a standard normal distribution, i.e, so that $F_\theta(X) \sim \mathcal{N}(0, I)$. In other words, we want F_θ to map the *true* data distribution to a standard normal, that is, when considered as a functional on probability distributions, the optimal reconstructor should reverse the optimal generator.

Formally, let $p_\theta(z|x)$ to denote the deterministic conditional distribution defined by F_θ, i.e., a delta function, so that $p_\theta(z) = \int p_\theta(z|x)p(x)\,dx$. We choose θ to minimize the cross entropy

$$H(Z, F_\theta(X)) = -\int p_0(z) \log p_\theta(z) dz = -\int p_0(z) \log \int p(x) p_\theta(z|x)\,dx\,dz, \tag{1}$$

where p_0 is the standard normal density. This cross entropy is minimized with respect to θ when $p_\theta(z) = p_0(z)$ [2] . Unfortunately, the integral on the right-hand side of (1) cannot usually be computed in closed form. We introduce an alternative optimization target in the form of a variational bound for $p_\theta(z)$, by introducing a variational distribution $q_\gamma(x|z)$. By Jensen's inequality, we have

$$-\log p_\theta(z) = -\log \int p_\theta(z|x)p(x)\frac{q_\gamma(x|z)}{q_\gamma(x|z)}\,dx \leq -\int q_\gamma(x|z) \log \frac{p_\theta(z|x)p(x)}{q_\gamma(x|z)}\,dx, \tag{2}$$

which we use to bound the cross-entropy in (1). In variational inference, strong parametric assumptions are typically made on q_γ. Importantly, we relax that assumption, instead representing q_γ implicitly as a deep generative model, enabling us to learn very complex distributions. The variational distribution $q_\gamma(x|z)$ plays exactly the same role as the generator in a GAN. We defer the details of how we handle implicit probability distributions to the next section.

In practice minimizing this bound is difficult if q_γ is specified implicitly. For instance, it is challenging to train a discriminator network that accurately estimates the unknown likelihood ratio $\log p(x)/q_\gamma(x|z)$, because $q_\gamma(x|z)$, as a conditional distribution, is much more peaked than the joint distribution $p(x)$, making it too easy for a discriminator to tell the two distributions apart. Intuitively, the discriminator in a GAN works well when it is presented a *difficult* pair of distributions to distinguish. To circumvent this problem, we introduce a second bound (all proofs in supplementary material):

$$-\int p_0(z)\log p_\theta(z) \leq \mathcal{O}(\gamma,\theta)$$

$$\mathcal{O}(\gamma,\theta) = \mathrm{KL}\left[q_\gamma(x|z)p_0(z) \,\|\, p_\theta(z|x)p(x)\right] - E\left[\log p_0(z)\right] + E\left[d(z,F_\theta(x))\right], \quad (3)$$

where all expectations are taken with respect to the joint distribution $p_0(z)q_\gamma(x|z)$. The second term does not depend on γ or θ, and is thus a constant, because $p_0(z)$ does neither depends on them nor on x. The function d denotes a loss function in representation space $\mathbb{R}^K$, such as ℓ_2 loss. The third term in (3) is then an autoencoder in representation space. To make this link explicit, we expand the expectation, assuming that we choose d to be ℓ_2 loss. This yields $E\left[d(z,F_\theta(x))\right] = \int p_0(z)\|z - F_\theta(G_\gamma(z))\|^2\,dz$. We can therefore interpret the third term of (3) as a regularization term that attempts to minimize the reconstruction error of an autoencoder on z. Unlike a standard autoencoder, however, rather than taking a *data item* as input and attempting to reconstruct it, we autoencode a *representation vector*. This makes a substantial difference in the interpretation and performance of the method, as we discuss in Section 4. For example, notice that we do not include a regularization weight on the autoencoder term in (3), because Proposition 1 below says that this is not needed to recover the data distribution without one. We thus did not include a regularization weight in our experiments.

Rather than minimizing the intractable cross entropy $H(Z,F_\theta(X))$, our goal in VEEGAN is to minimize the upper bound $\mathcal{O}$ with respect to γ and θ. Indeed, if the networks F_θ and G_γ are sufficiently powerful, then if we succeed in globally minimizing $\mathcal{O}$, we can guarantee that q_γ recovers the true data distribution. This statement is formalized in the following proposition.

Proposition 1. *Suppose that there exist parameters θ^*,γ^* such that $\mathcal{O}(\gamma^*,\theta^*) = H[p_0]$, where H denotes Shannon entropy. Then (γ^*,θ^*) minimizes $\mathcal{O}$, and further*

$$p_{\theta^*}(z) := \int p_{\theta^*}(z|x)p(x)\,dx = p_0(z), \quad \textit{and} \quad q_{\gamma^*}(x) := \int q_{\gamma^*}(x|z)p_0(z)\,dz = p(x).$$

Because neural networks are universal approximators, the conditions in the proposition can be achieved when the networks G and F are sufficiently powerful.

3.2 Learning with Implicit Probability Distributions

This subsection describes how to approximate $\mathcal{O}$ when we have implicit representations for q_γ and p_θ rather than explicit densities. In this case, we cannot optimize $\mathcal{O}$ directly, because the KL divergence in (3) depends on a density ratio which is unknown, both because q_γ is implicit and also because $p(x)$ is unknown. Following [4, 5], we estimate this ratio using a discriminator network $D_\omega(x,z)$ which we will train to encourage

$$D_\omega(z,x) = \log\frac{q_\gamma(x|z)p_0(z)}{p_\theta(z|x)p(x)}. \quad (4)$$

This will allow us to estimate $\mathcal{O}$ as

$$\hat{\mathcal{O}}(\omega,\gamma,\theta) = \frac{1}{N}\sum_{i=1}^N \mathcal{D}_\omega(z^i,x_g^i) + \frac{1}{N}\sum_{i=1}^N d(z^i,x_g^i), \quad (5)$$

where $(z^i,x_g^i) \sim p_0(z)q_\gamma(x|z)$. In this equation, note that x_g^i is a function of γ; although we suppress this in the notation, we do take this dependency into account in the algorithm. We use an auxiliary objective function to estimate ω. As mentioned earlier, we omit the entropy term $-E\left[\log p_0(z)\right]$ from $\hat{\mathcal{O}}$ as it is constant with respect to all parameters. In principle, any method for density ratio estimation could be used here, for example, see [8, 21]. In this work, we will use the logistic regression loss, much as in other methods for deep adversarial training, such as GANs [6], or for noise contrastive estimation [7]. We will train D_ω to distinguish samples from the joint distribution $q_\gamma(x|z)p_0(z)$ from $p_\theta(z|x)p(x)$. The objective function for this is

$$\mathcal{O}_{\text{LR}}(\omega,\gamma,\theta) = -E_\gamma\left[\log\left(\sigma\left(D_\omega(z,x)\right)\right)\right] - E_\theta\left[\log\left(1-\sigma\left(D_\omega(z,x)\right)\right)\right], \quad (6)$$

Algorithm 1 VEEGAN training

while not converged **do**
  for $i \in \{1 \dots N\}$ **do**
    Sample $z^i \sim p_0(z)$
    Sample $x_g^i \sim q_\gamma(x|z_i)$
    Sample $x^i \sim p(x)$
    Sample $z_g^i \sim p_\theta(z_g|x_i)$
  $g_\omega \leftarrow -\nabla_\omega \frac{1}{N} \sum_i \log \sigma\left(D_\omega(z^i, x_g^i)\right) + \log\left(1 - \sigma\left(D_\omega(z_g^i, x^i)\right)\right)$ ▷ Compute $\nabla_\omega \hat{\mathcal{O}}_{\text{LR}}$
  $g_\theta \leftarrow \nabla_\theta \frac{1}{N} \sum_i d(z^i, x_g^i)$ ▷ Compute $\nabla_\theta \hat{\mathcal{O}}$
  $g_\gamma \leftarrow \nabla_\gamma \frac{1}{N} \sum_i D_\omega(z^i, x_g^i) + \frac{1}{N} \sum_i d(z^i, x_g^i)$ ▷ Compute $\nabla_\gamma \hat{\mathcal{O}}$
  $\omega \leftarrow \omega - \eta g_\omega$; $\theta \leftarrow \theta - \eta g_\theta$; $\gamma \leftarrow \gamma - \eta g_\gamma$ ▷ Perform SGD updates for ω, θ and γ

where E_γ denotes expectation with respect to the joint distribution $q_\gamma(x|z)p_0(x)$ and E_θ with respect to $p_\theta(z|x)p(x)$. We write $\hat{\mathcal{O}}_{\text{LR}}$ to indicate the Monte Carlo estimate of $\mathcal{O}_{\text{LR}}$. Our learning algorithm optimizes this pair of equations with respect to γ, ω, θ using stochastic gradient descent. In particular, the algorithms aim to find a simultaneous solution to $\min_\omega \hat{\mathcal{O}}_{\text{LR}}(\omega, \gamma, \theta)$ and $\min_{\theta,\gamma} \hat{\mathcal{O}}(\omega, \gamma, \theta)$. This training procedure is described in Algorithm 1. When this procedure converges, we will have that $\omega^* = \arg\min_\omega \mathcal{O}_{\text{LR}}(\omega, \gamma^*, \theta^*)$, which means that D_{ω^*} has converged to the likelihood ratio (4). Therefore (γ^*, θ^*) have also converged to a minimum of $\mathcal{O}$.

4 Relationships to Other Methods

An enormous amount of attention has been devoted recently to improved methods for GAN training, and we compare ourselves to the most closely related work in detail.

BiGAN/Adversarially Learned Inference BiGAN [4] and Adversarially Learning Inference (ALI) [5] are two essentially identical recent adversarial methods for learning both a deep generative network G_γ and a reconstructor network F_θ. Likelihood-free variational inference (LFVI) [22] extends this idea to a hierarchical Bayesian setting. Like VEEGAN, all of these methods also use a discriminator $D_\omega(z, x)$ on the joint (z, x) space. However, the VEEGAN objective function $\mathcal{O}(\theta, \gamma)$ provides significant benefits over the logistic regression loss over θ and γ that is used in ALI/BiGAN, or the KL-divergence used in LFVI. In all of these methods, just as in vanilla GANs, the objective function depends on θ and γ only via the output $D_\omega(z, x)$ of the discriminator; therefore, if there is a mode of data space in which D_ω is insensitive to changes in θ and γ, there will be mode collapse. In VEEGAN, by contrast, the reconstruction term does not depend on the discriminator, and so can provide learning signal to γ or θ even when the discriminator is constant. We will show in Section 5 that indeed VEEGAN is dramatically less prone to mode collapse than ALI.

Adversarial Methods for Autoencoders A number of other recent methods have been proposed that combine adversarial methods and autoencoders, whether by explicitly regularizing the GAN loss with an autoencoder loss [1, 12], or by alternating optimization between the two losses [14]. In all of these methods, the autoencoder is over images, i.e., they incorporate a loss function of the form $\lambda d(x, G_\gamma(F_\theta(x)))$, where d is a loss function over images, such as pixel-wise ℓ_2 loss, and λ is a regularization constant. Similarly, variational autoencoders [11, 18] also autoencode images rather than noise vectors. Finally, the adversarial variational Bayes (AVB) [15] is an adaptation of VAEs to the case where the posterior distribution $p_\theta(z|x)$ is implicit, but the data distribution $q_\gamma(x|z)$, must be explicit, unlike in our work.

Because these methods autoencode data points, they share a crucial disadvantage. Choosing a good loss function d over natural images can be problematic. For example, it has been commonly observed that minimizing an ℓ_2 reconstruction loss on images can lead to blurry images. Indeed, if choosing a loss function over images were easy, we could simply train an autoencoder and dispense with adversarial learning entirely. By contrast, in VEEGAN we autoencode the noise vectors z, and

choosing a good loss function for a noise autoencoder is easy. The noise vectors z are drawn from a standard normal distribution, using an ℓ_2 loss on z is entirely natural — and does not, as we will show in Section 5, result in blurry images compared to purely adversarial methods.

5 Experiments

Quantitative evaluation of GANs is problematic because implicit distributions do not have a tractable likelihood term to quantify generative accuracy. Quantifying mode dropping is also not straightforward, except in the case of synthetic data with known modes. For this reason, several indirect metrics have recently been proposed to evaluate GANs specifically for their mode collapsing behavior [1, 16]. However, none of these metrics are reliable on their own and therefore we need to compare across a number of different methods. Therefore in this section we evaluate VEEGAN on several synthetic and real datasets and compare its performance against vanilla GANs [6], Unrolled GAN [16] and ALI [5] on five different metrics. Our results strongly suggest that VEEGAN does indeed resolve mode collapse in GANs to a large extent. Generally, we found that VEEGAN performed well with default hyperparameter values, so we did not tune these. Full details are provided in the supplementary material.

5.1 Synthetic Dataset

Mode collapse can be accurately measured on synthetic datasets, since the true distribution and its modes are known. In this section we compare all four competing methods on three synthetic datasets of increasing difficulty: a mixture of eight 2D Gaussian distributions arranged in a ring, a mixture of twenty-five 2D Gaussian distributions arranged in a grid and a mixture of ten 700 dimensional Gaussian distributions embedded in a 1200 dimensional space. This mixture arrangement was chosen to mimic the higher dimensional manifolds of natural images. All of the mixture components were isotropic Gaussians. For a fair comparison of the different learning methods for GANs, we use the same network architectures for the reconstructors and the generators for all methods, namely, fully-connected MLPs with two hidden layers. For the discriminator we use a single hidden layer MLP without dropout or normalization layers.

To quantify the mode collapsing behavior we report two metrics: We sample points from the generator network, and count a sample as *high quality*, if it is within three standard deviations of the nearest mode, for the 2D dataset, or within 10 standard deviations of the nearest mode, for the 1200D dataset. Then, we report the *number of modes captured* as the number of mixture components whose mean is nearest to at least one high quality sample. We also report the percentage of high quality samples as a measure of sample quality. We generate 2500 samples from each trained model and average the numbers over five runs. For the unrolled GAN, we set the number of unrolling steps to five as suggested in the authors' reference implementation.

As shown in Table 1, VEEGAN captures the greatest number of modes on all the synthetic datasets, while consistently generating higher quality samples. This is visually apparent in Figure 2, which plot the generator distributions for each method; the generators learned by VEEGAN are sharper and closer to the true distribution. This figure also shows why it is important to measure sample quality and mode collapse simultaneously, as either alone can be misleading. For instance, the GAN on the 2D ring has 99.3% sample quality, but this is simply because the GAN collapses all of its samples onto one mode (Figure 2b). On the other extreme, the unrolled GAN on the 2D grid captures almost all the modes in the true distribution, but this is simply because that it is generating highly dispersed samples (Figure 2i) that do not accurately represent the true distribution, hence the low sample quality. All methods had approximately the same running time, except for unrolled GAN, which is a few orders of magnitude slower due to the unrolling overhead.

5.2 Stacked MNIST

Following [16], we evaluate our methods on the stacked MNIST dataset, a variant of the MNIST data specifically designed to increase the number of discrete modes. The data is synthesized by stacking three randomly sampled MNIST digits along the color channel resulting in a 28x28x3 image. We now expect 1000 modes in this data set, corresponding to the number of possible triples of digits.

Table 1: Sample quality and degree of mode collapse on mixtures of Gaussians. VEEGAN consistently captures the highest number of modes and produces better samples.

	2D Ring		2D Grid		1200D Synthetic	
	Modes (Max 8)	**% High Quality Samples**	**Modes (Max 25)**	**% High Quality Samples**	**Modes (Max 10)**	**% High Quality Samples**
GAN	1	99.3	3.3	0.5	1.6	2.0
ALI	2.8	0.13	15.8	1.6	3	5.4
Unrolled GAN	7.6	35.6	23.6	16	0	0.0
VEEGAN	**8**	**52.9**	**24.6**	**40**	**5.5**	**28.29**

	Stacked-MNIST		CIFAR-10
	Modes (Max 1000)	KL	IvOM
DCGAN	99	3.4	0.00844 ± 0.002
ALI	16	5.4	$\mathbf{0.0067} \pm 0.004$
Unrolled GAN	48.7	4.32	0.013 ± 0.0009
VEEGAN	**150**	**2.95**	$\mathbf{0.0068} \pm 0.0001$

Table 2: Degree of mode collapse, measured by modes captured and the inference via optimization measure (IvOM), and sample quality (as measured by KL) on Stacked-MNIST and CIFAR. VEEGAN captures the most modes and also achieves the highest quality.

Again, to focus the evaluation on the difference in the learning algorithms, we use the same generator architecture for all methods. In particular, the generator architecture is an off-the-shelf standard implementation[2] of DCGAN [17]. For Unrolled GAN, we used a standard implementation of the DCGAN discriminator network. For ALI and VEEGAN, the discriminator architecture is described in the supplementary material. For the reconstructor in ALI and VEEGAN, we use a simple two-layer MLP for the reconstructor without any regularization layers. Finally, for VEEGAN we pretrain the reconstructor by taking a few stochastic gradient steps with respect to θ before running Algorithm 1. For all methods other than VEEGAN, we use the enhanced generator loss function suggested in [6], since we were not able to get sufficient learning signals for the generator without it. VEEGAN did not require this adjustment for successful training.

As the true locations of the modes in this data are unknown, the number of modes are estimated using a trained classifier as described originally in [1]. We used a total of 26000 samples for all the models and the results are averaged over five runs. As a measure of quality, following [16] again, we also report the KL divergence between the generator distribution and the data distribution. As reported in Table 2, VEEGAN not only captures the most modes, it consistently matches the data distribution more closely than any other method. Generated samples from each of the models are shown in the supplementary material.

5.3 CIFAR

Finally, we evaluate the learning methods on the CIFAR-10 dataset, a well-studied and diverse dataset of natural images. We use the same discriminator, generator, and reconstructor architectures as in the previous section. However, the previous mode collapsing metric is inappropriate here, owing to CIFAR's greater diversity. Even within one of the 10 classes of CIFAR, the intra-group diversity is very high compared to any of the 10 classes of MNIST. Therefore, for CIFAR it is inappropriate to assume, as the metrics of the previous subsection do, that each labelled class corresponds to a single mode of the data distribution.

Instead, we use a metric introduced by [16] which we will call the inference via optimization metric (IvOM). The idea behind this metric is to compare real images from the test set to the nearest

[2] `https://github.com/carpedm20/DCGAN-tensorflow`

generated image; if the generator suffers from mode collapse, then there will be some images for which this distance is large. To quantify this, we sample a real image x from the test set, and find the closest image that the GAN is capable of generating, i.e. optimizing the ℓ_2 loss between x and generated image $G_\gamma(z)$ with respect to z. If a method consistently attains low MSE, then it can be assumed to be capturing more modes than the ones which attain a higher MSE. As before, this metric can still be fooled by highly dispersed generator distributions, and also the ℓ_2 metric may favour generators that produce blurry images. Therefore we will also evaluate sample quality visually. All numerical results have been averaged over five runs. Finally, to evaluate whether the noise autoencoder in VEEGAN is indeed superior to a more traditional data autoencoder, we compare to a variant, which we call VEEGAN +DAE, that uses a data autoencoder instead, by simply replacing $d(z, F_\theta(x))$ in $\mathcal{O}$ with a data loss $\|x - G_\gamma(F_\theta(x))\|_2^2$.

As shown in Table 2, ALI and VEEGAN achieve the best IvOM. Qualitatively, however, generated samples from VEEGAN seem better than other methods. In particular, the samples from VEEGAN +DAE are meaningless. Generated samples from VEEGAN are shown in Figure 3b; samples from other methods are shown in the supplementary material. As another illustration of this, Figure 3 illustrates the IvOM metric, by showing the nearest neighbors to real images that each of the GANs were able to generate; in general, the nearest neighbors will be more semantically meaningful than randomly generated images. We omit VEEGAN +DAE from this table because it did not produce plausible images. Across the methods, we see in Figure 3 that VEEGAN captures small details, such as the face of the poodle, that other methods miss.

Figure 2: Density plots of the true data and generator distributions from different GAN methods trained on mixtures of Gaussians arranged in a ring (top) or a grid (bottom).

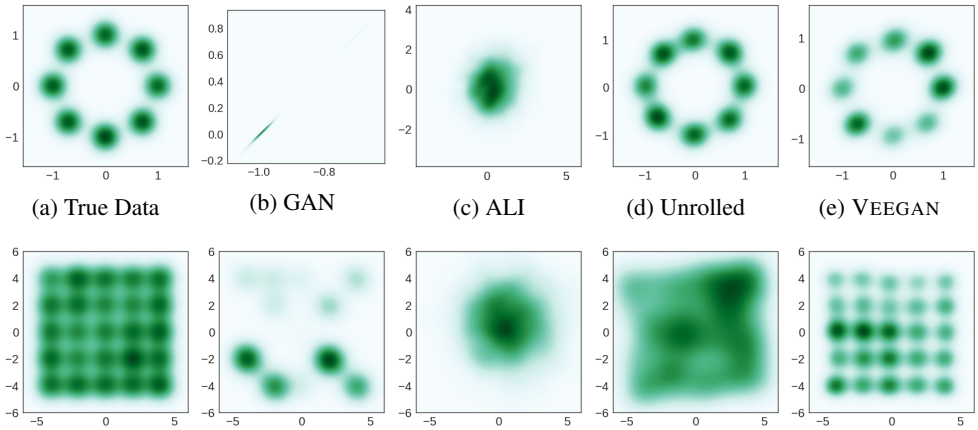

(a) True Data (b) GAN (c) ALI (d) Unrolled (e) VEEGAN

(f) True Data (g) GAN (h) ALI (i) Unrolled (j) VEEGAN

6 Conclusion

We have presented VEEGAN, a new training principle for GANs that combines a KL divergence in the joint space of representation and data points with an autoencoder over the representation space, motivated by a variational argument. Experimental results on synthetic data and real images show that our approach is much more effective than several state-of-the art GAN methods at avoiding mode collapse while still generating good quality samples.

Acknowledgement

We thank Martin Arjovsky, Nicolas Collignon, Luke Metz, Casper Kaae Sønderby, Lucas Theis, Soumith Chintala, Stanisław Jastrzębski, Harrison Edwards and Amos Storkey for their helpful comments. We would like to specially thank Ferenc Huszár for insightful discussions and feedback.

Figure 3: Sample images from GANs trained on CIFAR-10. Best viewed magnified on screen.

(a) Generated samples nearest to real images from CIFAR-10. In each of the two panels, the first column are real images, followed by the nearest images from DCGAN, ALI, Unrolled GAN, and VEEGAN respectively.

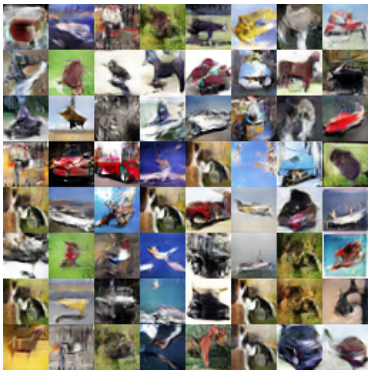

(b) Random samples from generator of VEEGAN trained on CIFAR-10.

References

[1] Che, Tong, Li, Yanran, Jacob, Athul Paul, Bengio, Yoshua, and Li, Wenjie. Mode regularized generative adversarial networks. In *International Conference on Learning Representations (ICLR)*, volume abs/1612.02136, 2017.

[2] Cover, Thomas M and Thomas, Joy A. *Elements of information theory*. John Wiley & Sons, 2012.

[3] Diggle, Peter J. and Gratton, Richard J. Monte carlo methods of inference for implicit statistical models. *Journal of the Royal Statistical Society. Series B (Methodological)*, 46(2):193–227, 1984. ISSN 00359246. URL `http://www.jstor.org/stable/2345504`.

[4] Donahue, Jeff, Krähenbühl, Philipp, and Darrell, Trevor. Adversarial feature learning. In *International Conference on Learning Representations (ICLR)*, 2017.

[5] Dumoulin, Vincent, Belghazi, Ishmael, Poole, Ben, Mastropietro, Olivier, Lamb, Alex, Arjovsky, Martin, and Courville, Aaron. Adversarially learned inference. In *International Conference on Learning Representations (ICLR)*, 2017.

[6] Goodfellow, Ian J., Pouget-Abadie, Jean, Mirza, Mehdi, Xu, Bing, Warde-Farley, David, Ozair, Sherjil, Courville, Aaron C., and Bengio, Yoshua. Generative adversarial nets. In *Advances in Neural Information Processing Systems*, pp. 2672–2680, 2014.

[7] Gutmann, Michael U. and Hyvarinen, Aapo. Noise-contrastive estimation of unnormalized statistical models, with applications to natural image statistics. *Journal of Machine Learning Research*, 13:307–361, 2012.

[8] Gutmann, M.U. and Hirayama, J. Bregman divergence as general framework to estimate unnormalized statistical models. In *Proc. Conf. on Uncertainty in Artificial Intelligence (UAI)*, pp. 283–290, Corvallis, Oregon, 2011. AUAI Press.

[9] Gutmann, M.U., Dutta, R., Kaski, S., and Corander, J. Likelihood-free inference via classification. *arXiv:1407.4981*, 2014.

[10] Kingma, Diederik P and Welling, Max. Auto-encoding variational bayes. *arXiv preprint arXiv:1312.6114*, 2013.

[11] Kingma, D.P. and Welling, M. Auto-encoding variational bayes. In *International Conference on Learning Representations (ICLR)*, 2014.

[12] Larsen, Anders Boesen Lindbo, Sønderby, Søren Kaae, Larochelle, Hugo, and Winther, Ole. Autoencoding beyond pixels using a learned similarity metric. In *International Conference on Machine Learning (ICML)*, 2016.

[13] Liu, Ziwei, Luo, Ping, Wang, Xiaogang, and Tang, Xiaoou. Deep learning face attributes in the wild. In *Proceedings of International Conference on Computer Vision (ICCV)*, 2015.

[14] Makhzani, Alireza, Shlens, Jonathon, Jaitly, Navdeep, and Goodfellow, Ian J. Adversarial autoencoders. Arxiv preprint 1511.05644, 2015. URL `http://arxiv.org/abs/1511.05644`.

[15] Mescheder, Lars M., Nowozin, Sebastian, and Geiger, Andreas. Adversarial variational bayes: Unifying variational autoencoders and generative adversarial networks. *ArXiv*, abs/1701.04722, 2017. URL `http://arxiv.org/abs/1701.04722`.

[16] Metz, Luke, Poole, Ben, Pfau, David, and Sohl-Dickstein, Jascha. Unrolled generative adversarial networks. *arXiv preprint arXiv:1611.02163*, 2016.

[17] Radford, Alec, Metz, Luke, and Chintala, Soumith. Unsupervised representation learning with deep convolutional generative adversarial networks. *arXiv preprint arXiv:1511.06434*, 2015.

[18] Rezende, Danilo Jimenez, Mohamed, Shakir, and Wierstra, Daan. Stochastic backpropagation and approximate inference in deep generative models. In *Proceedings of The 31st International Conference on Machine Learning*, pp. 1278–1286, 2014.

[19] Salimans, Tim, Goodfellow, Ian J., Zaremba, Wojciech, Cheung, Vicki, Radford, Alec, and Chen, Xi. Improved techniques for training gans. *CoRR*, abs/1606.03498, 2016. URL `http://arxiv.org/abs/1606.03498`.

[20] Sønderby, Casper Kaae, Caballero, Jose, Theis, Lucas, Shi, Wenzhe, and Huszár, Ferenc. Amortised map inference for image super-resolution. *arXiv preprint arXiv:1610.04490*, 2016.

[21] Sugiyama, M., Suzuki, T., and Kanamori, T. *Density ratio estimation in machine learning*. Cambridge University Press, 2012.

[22] Tran, D., Ranganath, R., and Blei, D. M. Deep and Hierarchical Implicit Models. *ArXiv e-prints*, 2017.

[23] Zhu, Jun-Yan, Park, Taesung, Isola, Phillip, and Efros, Alexei A. Unpaired image-to-image translation using cycle-consistent adversarial networks. *arXiv preprint arXiv:1703.10593*, 2017.

A Proof of Lower Bound

This appendix completes the proof of the bound in the text that

$$H(Z, F_\theta(X)) = -\int p_0(z) \log p_\theta(z) dz \leq \mathcal{O}(\gamma, \theta) \tag{7}$$

where p_0 is the standard normal density, and $p_\theta(z) = \int p_\theta(z|x)p(x)\,dx$. As described in the text, introducing a a variational distribution $q_\gamma(x|z)$ yields

$$-\int p_0(z) \log p_\theta(z)\,dz \leq -\iint p_0(z) q_\gamma(x|z) \log \frac{p_\theta(z|x)p(x)}{q_\gamma(x|z)}\,dx\,dz. \tag{8}$$

Starting from (8), we obtain a new upper bound by adding a trivial KL divergence to the right hand side of the above inequality

$$\begin{aligned} -\int p_0(z) \log p_\theta(z)\,dz &\leq -\iint p_0(z) q_\gamma(x|z) \log \frac{p_\theta(z|x)p(x)}{q_\gamma(x|z)}\,dx\,dz \\ &= \iint p_0(z) q_\gamma(x|z) \log \frac{q_\gamma(x|z)}{p_\theta(z|x)p(x)}\,dx\,dz + \int p_0(z) \log \frac{p_0(z)}{p_0(z)}\,dz \end{aligned} \tag{9}$$

Now for the upper term in the KL, we have that

$$\int p_0(z) \log p_0(z)\,dz = \int p_0(z) \log p_0(z) \left(\int q_\gamma(x|z)\,dx \right) dz = \iint p_0(z) q_\gamma(x|z) \log p_0(z)\,dx\,dz.$$

Combining with (9) yields

$$\begin{aligned} H(Z, F_\theta(X)) &\leq \iint p_0(z) q_\gamma(x|z) \log \frac{q_\gamma(x|z)}{p_\theta(z|x)p(x)}\,dx\,dz + \iint p_0(z) q_\gamma(x|z) \log p_0(z)\,dx\,dz \\ &\quad - \int p_0(z) \log p_0(z)\,dz \\ &= \iint p_0(z) q_\gamma(x|z) \log \frac{q_\gamma(x|z)p_0(z)}{p_\theta(z|x)p(x)}\,dx\,dz - \int p_0(z) \log p_0(z)\,dz \\ &= \mathrm{KL}\left[q_\gamma(x|z)p_0(z) \,\|\, p_\theta(z|x)p(x)\right] - \int p_0(z) \log p_0(z)\,dz \end{aligned}$$

Since the loss function d is nonnegative, we further have

$$0 \leq \int p_0(z) d(z, F_\theta(G_\gamma(z)))\,dz = \iint p_0(z) q_\gamma(x|z) d(z, F_\theta(x))\,dx\,dz = E\left[d(z, F_\theta(x))\right]$$

so that

$$\begin{aligned} H(Z, F_\theta(X)) &\leq \mathrm{KL}\left[q_\gamma(x|z)p_0(z) \,\|\, p_\theta(z|x)p(x)\right] - \int p_0(z) \log p_0(z)\,dz + E\left[d(z, F_\theta(x))\right] \\ &:= \mathcal{O}(\gamma, \theta), \end{aligned} \tag{10}$$

which completes the proof.

B Proof of Proposition 1

Proposition 2. *Suppose that there exist parameters θ^*, γ^* such that $\mathcal{O}(\gamma^*, \theta^*) = H[p_0]$, where H denotes Shannon entropy. Then (γ^*, θ^*) minimizes $\mathcal{O}$, and we further have that*

$$\begin{aligned} p_{\theta^*}(z) &:= \int p_{\theta^*}(z|x)p(x)\,dx = p_0(z) \\ q_{\gamma^*}(x) &:= \int q_{\gamma^*}(x|z)p_0(z)\,dz = p(x). \end{aligned}$$

Proof. From information theory, we know that $\mathrm{KL}\left[q_\gamma(x|z)p_0(z) \,\|\, p_\theta(z|x)p(x)\right] \geq 0$. Additionally, we have that $E\left[d(z, F_\theta(x))\right] \geq 0$, as shown in the previous appendix. Moreover, by definition of $E\left[\right]$ in the proposition,

$$\begin{aligned} -E\left[\log p_0(z)\right] &= -\iint p_0(z)q_\gamma(x|z)\log p_0(z)\,dzdx = -\int p_0(z)\log p_0(z)\,dz \int q_\gamma(x|z)\,dx \\ &= -\int p_0(z)\log p_0(z)\,dz, \end{aligned}$$

which is the definition of the Shannon entropy $H[p_0]$ of p_0.

This implies that

$$\begin{aligned} \mathcal{O}(\gamma,\theta) &= \mathrm{KL}\left[q_\gamma(x|z)p_0(z) \,\|\, p_\theta(z|x)p(x)\right] - E\left[\log p_0(z)\right] + E\left[d(z, F_\theta(x))\right] \\ &\geq -E\left[\log p_0(z)\right] \\ &= H[p_0]. \end{aligned}$$

This bound is attained with equality when $q_\gamma(x|z)p_0(z) = p_\theta(z|x)p(x)$, and when F_θ inverts G_γ on the data distribution, i.e., when $F_\theta(G_\gamma(z)) = z$ for all z. (Note that this statement does not require G to be invertible outside of its range.)

Now, if $\mathcal{O}(\gamma^*, \theta^*) = H[p_0]$, subtracting the entropy from both sides implies that $\mathrm{KL}\left[q_\gamma(x|z)p_0(z) \,\|\, p_\theta(z|x)p(x)\right] = 0$. Because the optimum of the KL divergence is unique, we then have that $q_{\gamma^*}(x|z)p_0(z) = p_{\theta^*}(z|x)p(x)$.

Integrating both sides over x yields the first equality in the proposition, and integrating over z yields the second. □

C Discriminator Architecture for ALI and VEEGAN

When using ALI and VEEGAN, the original DCGAN discriminator needs to be augmented in order allow it to operate on pairs of images and noise vectors. In order to achieve this, we flatten the final convolutional layer of DCGAN's discriminator and concatenate it with the input noise vector. Afterwards, we run the concatenation through a hidden layer, and then compute $D_\omega(z, x)$ through a linear transformation.

Table 3: ALI and VEEGAN Discriminator Architecture.

Operation	**#Output**	**BN?**	**Activation**
$D_\omega(x)$			
Conv	64	False	Leaky ReLU
Conv	128	True	Leaky ReLU
Conv	256	True	Leaky ReLU
Conv	512	True	Leaky ReLU
Flatten	-	-	-
$\sigma(D_\omega(z, x))$	Concatenate $D_\omega(x)$ and z along the first axis.		
Fully Connected	512	False	Leaky ReLU
Fully Connected	1	False	Sigmoid

D Inference

While not the focus of this work, our method can also be used for inference as in the case of ALI and BiGAN models. Figure 4 shows an example of inference on MNIST. The top row samples are from the dataset. We extract the latent representation vector for each of the real images by running them through the trained reconstructor and then use the resulting vector in the generator to get the generated samples shown in the bottom row of the figure.

Figure 4: VEEGAN method can be used like ALI to perform inference. The means output from the reconstructor network for the real images in the top row are used as the latent features to samples the generated images in the bottom row.

E Adversarial Methods for Autoencoders

In order to quantify contrast the effect of autoencoding of noise in VEEGAN with autoencoding of data in DAE methods [1, 12] we train DAE version of VEEGAN by simply using the reconstructor network as an inference network. As mentioned before, careful tuning of the weighing parameter λ is needed to ensure that the ℓ_2 loss is only working as a regularizer. Therefore, we run a parameter sweep for λ. As shown in figure 5 we were not able to obtain any meaningful images for any of the tested values.

Figure 5: CIFAR 10 samples from GANs with data Autoencoders. We did a parameter sweep over the value of λ but were unable to generate any meaningful images for any of the values. Figure 5d is generated entirely from the ℓ_2 loss.

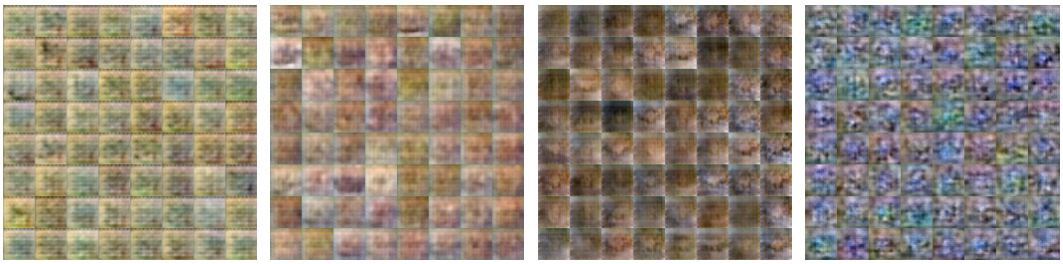

(a) $\lambda = 0.007$ (b) $\lambda = 0.01$ (c) $\lambda = 0.05$ (d) Only ℓ_2

F Stacked MNIST Qualitative Results

Qualitative results from the Stacked MNIST dataset for all the 4 methods.

Figure 6: Samples from trained models for Stacked MNIST dataset.

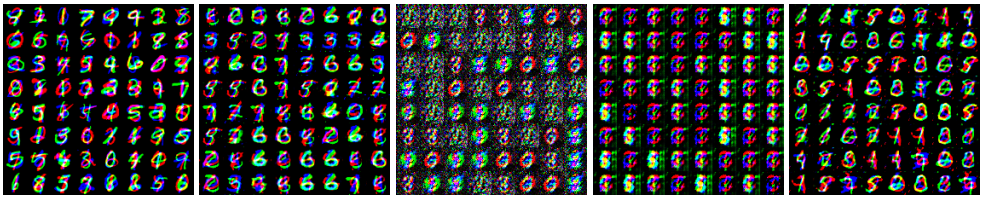

(a) True Data (b) DCGAN (c) ALI (d) Unrolled (e) VEEGAN

G CelebA Random Sample from ALI and VEEGAN

Additionally, we compared ALI and VEEGAN models on the much bigger CelebA dataset [13] of faces. Our goal is to test how robust each method is when used without extensive tuning of model

architecture and hyperparameters on a new dataset. Therefore we use the same model architectures and hyperparameters as we did on the CIFAR-10 data. While ALI failed to produce any meaningful images, VEEGAN generates high quality images of faces. Please note that this does not mean that ALI fails on CelebA in general. Indeed, as [5] show, given higher capacity reconstructor and discriminator with the right hyperparameters, it is possible to generate good quality images on this dataset. Rather, this experiment only suggests that for the simple network that we use for Stacked MNIST and CIFAR experiments, VEEGAN learning method was able to produce reasonable images without any further tuning or hyper parameter search.

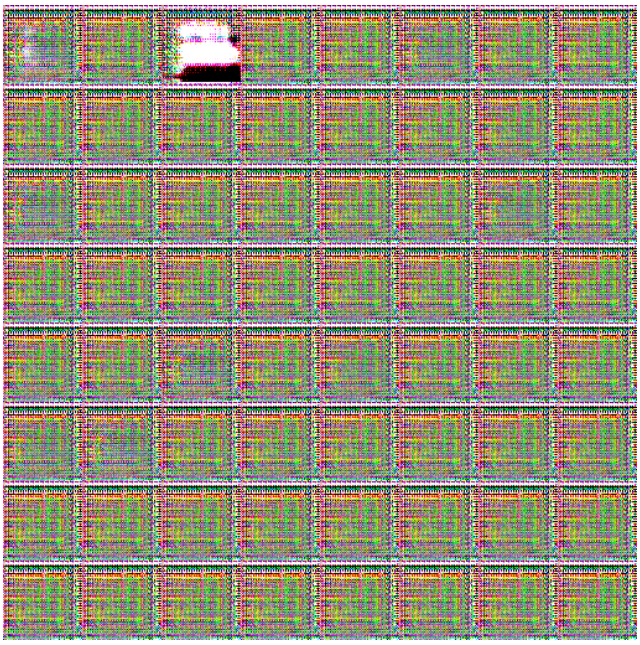

Figure 7: ALI on CelebA with simple DCGAN architecture and without tweaking of hyperparameters.

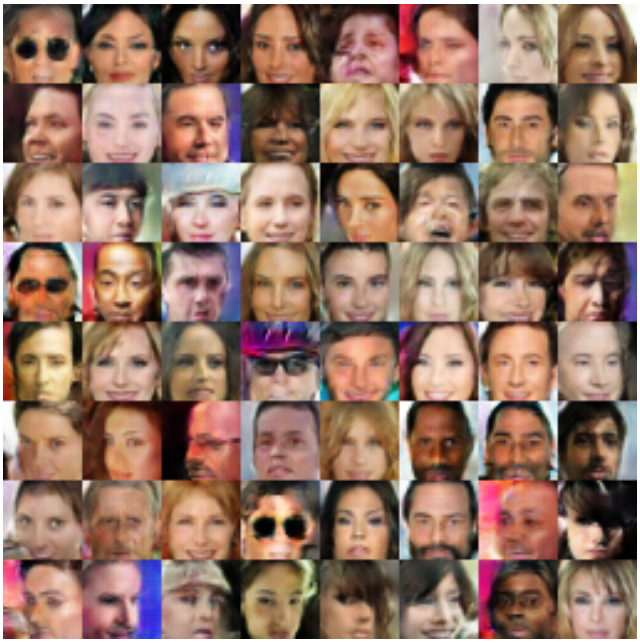

Figure 8: VEEGAN on CelebA with simple DCGAN architecture and default hyperparameters.

H CIFAR 10 Random Sample from VEEGAN

Randomly generated samples for CIFAR 10 dataset for all the 4 methods.

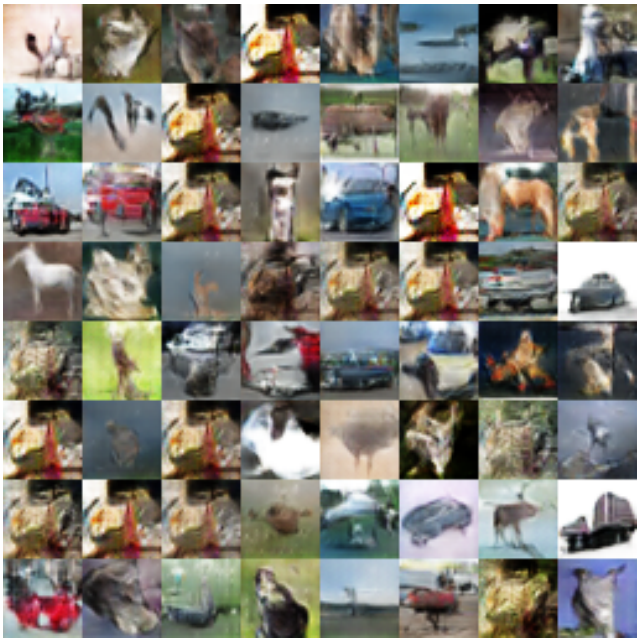

Figure 9: DCGAN on CIFAR 10 Dataset

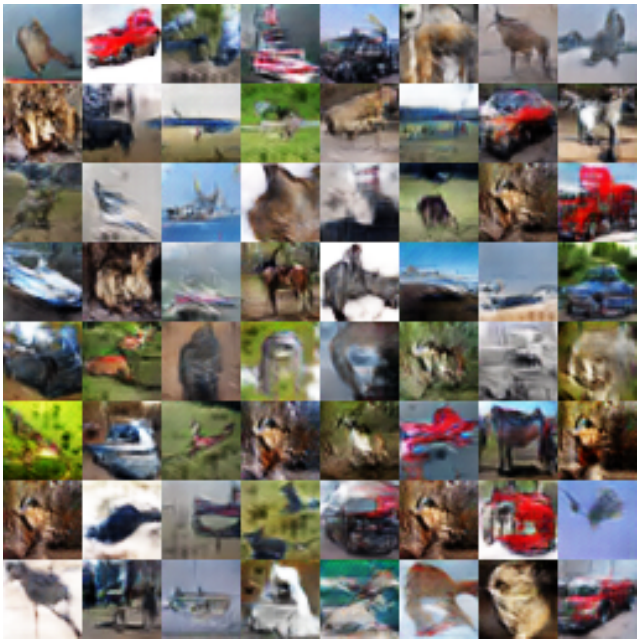

Figure 10: ALI on CIFAR 10 Dataset

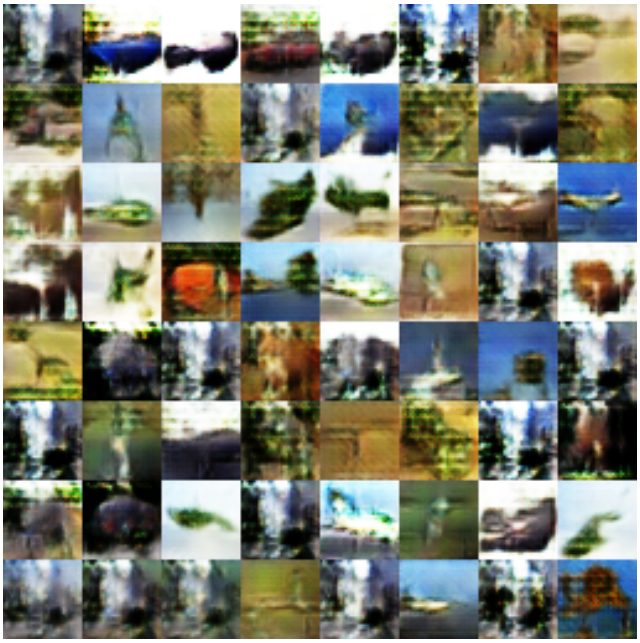

Figure 11: Unrolled GAN on CIFAR 10 Dataset

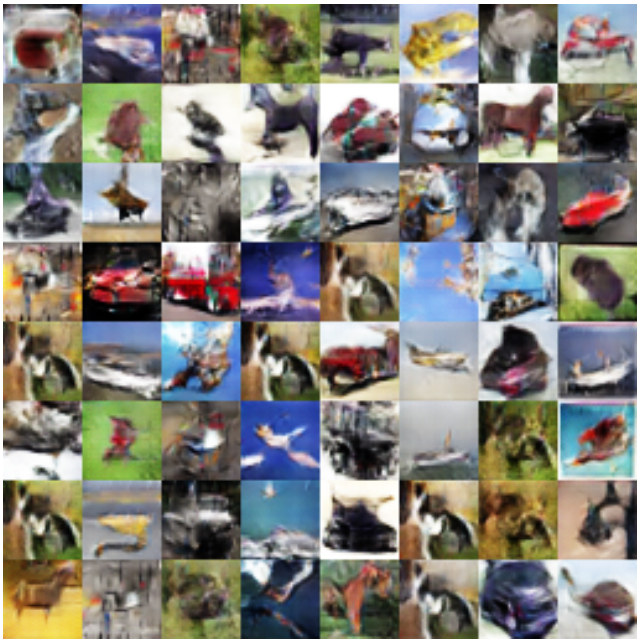

Figure 12: VEEGAN on CIFAR 10 Dataset